

Hafnium oxide based NEMS fabrication



Andrea ELISEI

Advanced NEMS Laboratory
Ecole Polytechnique Federale de Lausanne

Under the direction of Prof. Luis Guillermo VILLANUEVA
and supervisor Daniel MORENO

A thesis submitted for the degree of
Master of Science in Microengineering

Lausanne, 30th July 2021

Acknowledgments

I would like to express my profound gratitude to my supervisor Daniel Moreno, one of the nicest and most helpful people I have ever met apart from my family and close friends. I measure how lucky I have been to work with someone who complements my flaws, being supportive even in the many failures that we faced, and always pushing me forward.

I would like to thank Prof. Luis Guillermo Villanueva for having been such a good supervisor. His advice and supervision made me learn a lot during these last few months. He always made sure that I had all the tools and knowledge to carry out the project which will remain the culmination of my years of study.

It was an honor to be part of the ANEMS group with all these wonderful people that I shared great times with. My gratitude also goes to each of them as they all helped me at one point or another.

Last but certainly not least, I will be eternally grateful to my mother, my father, and more generally all my family and close friends without whom I would not be here writing this thesis of which I am so proud.

Thank you.

Andrea Elisei

Contents

1	Introduction	2
1.1	What is Flexoelectricity ?	3
1.2	Context and objective of the thesis	3
2	Microfabrication of HfO₂ flexoelectric actuators	4
2.1	Process flow	4
2.2	Bottom electrode liftoff	6
2.3	Dielectric deposition and top electrode evaporation	9
2.4	Top electrode patterning	10
2.5	Al pads liftoff and dicing	14
2.6	Actuators patterning	15
2.7	Actuators release	19
2.8	Measurements	20
3	HfO₂ crystallization	21
3.1	What is crystallization ?	21
3.2	Crystallization process	22
3.3	Crystallization results	23
4	Conclusion	25
	References	26
	Appendix	28

1 Introduction

On a daily basis, Microelectromechanical Systems (MEMS) are commonly used in sensors, accelerometers, actuators and serves communication, automotive, biomedical, and many more fields of applications. No wonder why these moving microscopic electrical devices are ubiquitous in our day-to-day life.

This journey started in 1947 with the invention of the first transistor to replace the vacuum-tube triode, which had both much bigger size and power consumption. It's then in 1965 that the now-famous Gordon Moore observed the basis of its "Moore's Law": the quantity of transistors per square inch on integrated circuits has been doubling every 18 months. His conclusion was that in the future, the technology would be focusing on smaller, not bigger, to improve [2].

If we believe that statement, then the Nanoelectromechanical Systems (NEMS) would be the natural successors of MEMS. Today, these devices of an order of magnitude lower are being studied in the research environment. Despite the many counterparts such as the difficulty in their fabrication and in their integration in larger systems, they stand for very good sensors and represent a link between classical and quantum mechanics.

Going always smaller comes with a massive challenge. It's getting harder and harder to actuate and sense the motion of the systems. To do so, numerous physical phenomenons are used in MEMS such as magnetic and electrostatic forces, piezoelectricity, piezoresistivity, and many more. The nanoscale scalability of the techniques used at the microscale is not always possible, even if the theory supports it. Take the case of piezoelectricity: it shows advantages such as low power consumption, straightforward integration, and a very low flexural rigidity, due to the decreasing device thickness, which allows for very small resolutions. But this is still not widely used due to the very challenging fabrication of high-quality piezoelectric thin film at the nanoscale.

An alternative to piezoelectricity is flexoelectricity due to its great advantages at the nanoscale, such as a coefficient unrelated to the film thickness and the fact that it doesn't need a shift of the neutral axis of the beam to generate a curvature. As of today, the potential substitute is undergoing research in many groups to study its characteristics in NEMS. Depending on the results, maybe some-day this phenomenon will be used way beyond the academic environment.

In this thesis, the challenging fabrication of flexoelectric NEMS actuators will be discussed. Firstly, the goal is to get a better understanding of the many steps that take place in the microfabrication of cantilevers based on hafnium oxide (HfO_2), a promising dielectric in the flexoelectric research. Many issues will be encountered and investigated to make sure that the process flow is optimized. On another hand, we will also be interested in the crystallization of HfO_2 thin films. Hopefully, these results will allow for a better understanding of the material's behavior and help in the characterization of HfO_2 's properties at the nanoscale.

1.1 What is Flexoelectricity ?

The flexoelectric effect is an electromechanical phenomenon that describes the coupling between the electric polarization and the mechanical strain gradient. Unlike piezoelectricity which only exists in non-centrosymmetric lattice materials, flexoelectricity is present in every dielectric. Although its effect is generally overlooked due to its very low impact in most situations, at the nanoscale it becomes significant or even dominant in few cases. To support this point, the constitutive equations for the electrical polarization P and for the stress σ are as follow [3] :

$$P = \chi E + \mu \frac{\partial \varepsilon}{\partial x}, \quad (1)$$

$$\sigma = c\varepsilon + \frac{\mu}{\chi} \frac{\partial P}{\partial x}, \quad (2)$$

$$\mu \equiv \chi f. \quad (3)$$

In Equations (1) and (2), the flexoelectricity manifests itself in the right side term. Obviously, it is always influenced by the flexoelectric coefficient μ which is obtained by the multiplication of the dielectric susceptibility χ with f the flexocoupling tensor. The other terms are quite common: E is the electrical field, ε is the strain and c is the elastic constant.

The flexoelectricity phenomenon was first theorized back in the early 1960s but it's only in 1981 that Indenbom et al. first expressed the term "flexoelectricity" to name it [4]. Some of the flexoelectric-based devices possible applications are nanocantilevers [5], energy harvesting [6] and nano/microsensors [7].

1.2 Context and objective of the thesis

This thesis is part of the natural successor project to the doctoral research of Dr. Kaitlin Howell. A part of her study was about characterizing the flexoelectric coefficient of amorphous hafnium oxide [1]. Currently a doctoral student in the Advanced NEMS group, Daniel Moreno took over the future of this subject. One of his objectives is to characterize the flexoelectric coefficient in doped and crystallized HfO_2 .

To do so, new devices need to be fabricated. The goal of this thesis is to go through all the steps of the process flow inspired by the one from Kaitlin Howell's thesis [1]. As said before, the fabrication of nanostructures is very complicated, many issues can emerge. This document aims to transcribe all the difficulties that have been encountered during the last semester and the solutions that have been found to build a process flow as strong and reliable as possible.

On the other hand, some crystallization researches and tests have been carried out to determine the viable annealing parameters to apply to HfO_2 in order to successfully fabricate the structures that will be used to characterize the impact of crystallization on the flexoelectric properties of hafnium oxide.

2 Microfabrication of HfO_2 flexoelectric actuators

In this first section, we study the fabrication of flexoelectric nanoactuators. Our design consists of a large variety of cantilevers, made by caging an interlayer of hafnium oxide between two platinum (Pt) electrodes. The general idea of the process flow is discussed to get a better understanding of the expected results. Then each major step constituting it is described more in detail with the objective to transcribe the specific parameters and difficulties that have been encountered during each one of these processes.

2.1 Process flow

In the future, various types of structures will be needed to characterize the effect of any changes in the HfO_2 properties on its flexoelectric coefficient. The global objective is then to come up with a strong, reliable, and simple process flow that is robust enough that it doesn't need to be totally redesigned every time we modify a parameter of the desired final device. Obviously, we took inspiration from Kaitlin Howell's process flow to build ours [1]. The challenge that exists in taking over someone else's project is to understand their ideas and thoughts. Of course, it helps to have access to their resources, but it is often complicated to realize what could go wrong during the process and how it could. It's for this reason that this is essential to go over the whole fabrication once to get a better understanding of it.

The schematics of the process flow main steps are shown in figure 1. The dicing step comes after the aluminum (Al) pads liftoff, so every step done before then is performed at the wafer level. This allows to quicken the fabrication compared to executing chip by chip fabrication only, but with the last two steps being done at the chip level we are still free to maximize the variety of actuators that we can fabricate.

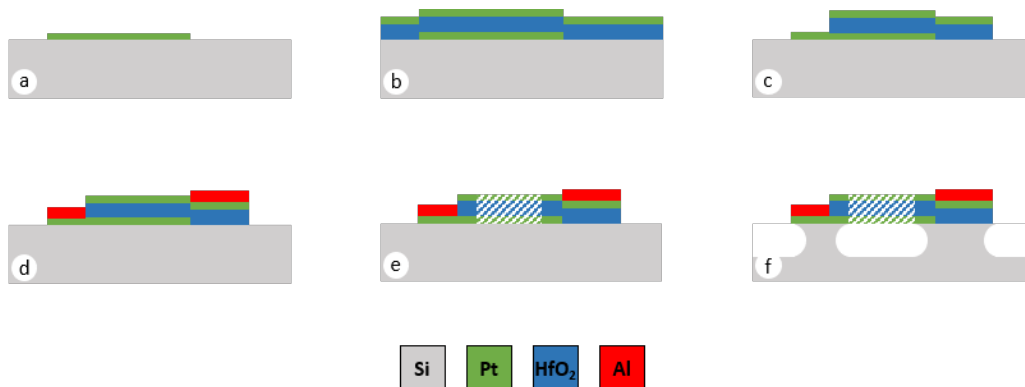


Figure 1: Main steps schematic (side view) of the device's process flow. (a) Bottom electrode liftoff; (b) Dielectric deposition and top electrode evaporation; (c) Top electrode patterning; (d) Al pads liftoff and wafer dicing; (e) Actuators patterning; (f) Actuators release. The hatched area is where the cantilevers are located.

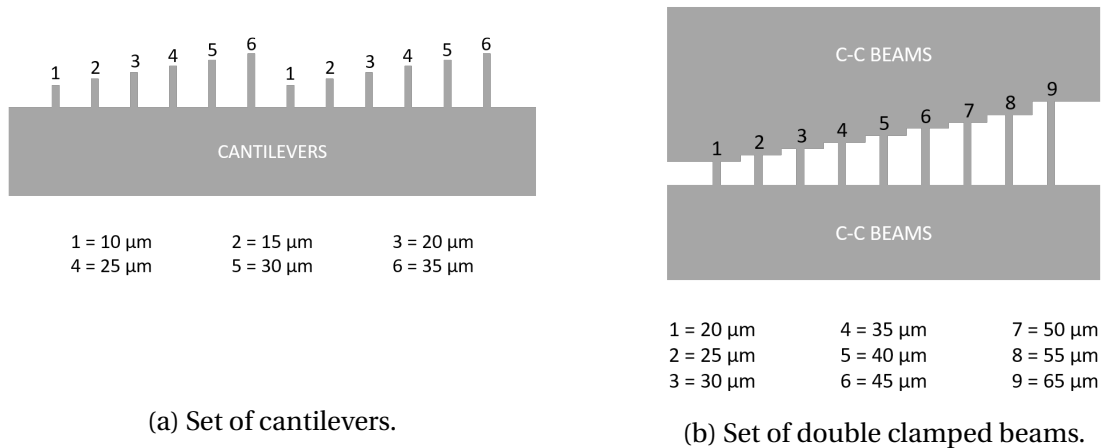


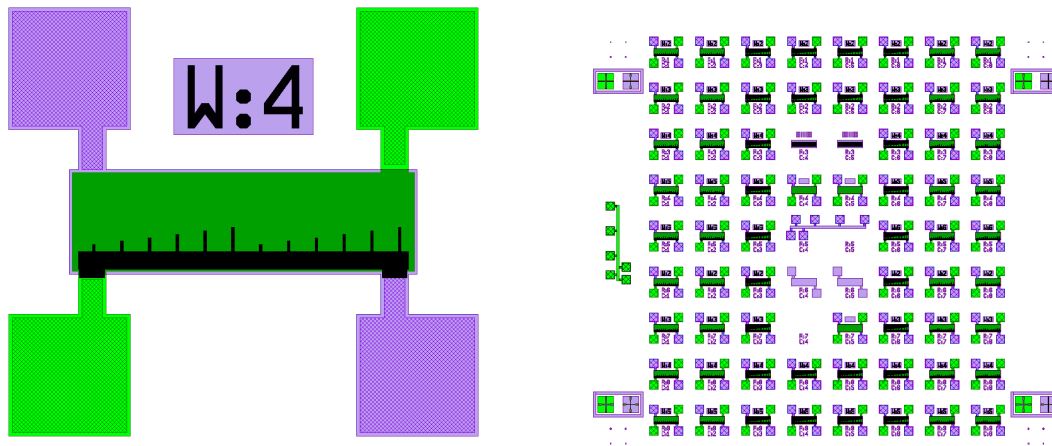
Figure 2: Schematic of beams lengths in the two types of actuators that can be found in the devices. This sizes stay the same no matter the width of the beams.

As the goal of the main project is the characterization of the flexoelectric effect and to show how it might be influenced by many parameters such as the design, the dielectric film thickness, the doping, or the crystallinity, there will be various models of cantilevers. Sets of multiple cantilevers or double clamped beams will be etched in the stack made by the top electrode, the dielectric, and the bottom electrode. These sets will be of diverse width and the beams constituting it will be of diverse length as shown in figure 2.

The current design patterns devices all over the substrate. A single wafer will provide 24 individually numbered chips after it gets diced and each of these chips has an array of structures of 9 rows and 8 columns. In reality, some of them are only used to test the proper functioning of the different parts of the system (e.g. the resistivity of the bottom electrode). In conclusion, each 15 x 15 mm chip contains a set of 62 study-dedicated structures as illustrated in figure 3b.

In figure 3a, a layout of a final structure can be seen. In the full design, each one of them is labeled according to its position in the array. Above the electrode, there is also a number that accounts for the width of the beams in the etched set. The idea is that the bottom electrode (in purple) and the top electrode (in green) overlap in the rectangle that forms in the center to create the stack of the three films that will constitute our actuators (in black). In each corner, there's a square that allows us to deposit the aluminum pads. Two of them will be evaporated on the bottom electrode (checkered in purple) and two of them will be evaporated on the top electrode (checkered in green). They allow protecting the thin films from the needles that will pinch through during the electrical measurements on the devices.

Now that we have a better understanding of the desired results and that we saw the general fabrication principles of our devices, we can deep dive into the development of the specifics.



(a) Example of an electrode mask design. The Pt bottom electrode is colored in purple and the Pt top electrode, which is covering the HfO_2 , is colored in green.

(b) Chip design. Many structures can be observed, as well as test structures (especially around the center).

Figure 3: Mask designs made on Clewin of the electrodes on the left and of the distribution on a chip on the right.

2.2 Bottom electrode liftoff

This fabrication process is mostly based on the principle of the bottom-up approach. It consists of starting from a bulk substrate and growing structures on it to obtain the final device. In this case, we use high resistive silicon (Si) wafers of 10 centimeters in diameter and about 500 micrometers in thickness. Compared to a top-bottom approach which is more based on etching through the initial substrate, the bottom-up is more desirable in nanofabrication because the quality of the obtained structures is much better. This is mostly since the processes are more reliable, leading to more homogeneous film depositions and fewer defects [8].

The liftoff principle is fairly easy to understand. The desired pattern is designed in photoresist on the substrate thanks to photolithography, then a film of the target material is deposited all over it. In the end, the sacrificial layer is removed, leaving on the surface of the substrate only the material that has stuck to it through the openings of the photoresist. This working principle is shown in picture 4.

Obviously, the first step is photolithography. In this case, it begins by stacking a 1.1 micrometers film of AZ 1512 onto a 480 nanometers deposition of LOR. This bi-layer allows to elevate the AZ 1512 film, which is the one that will pattern the bottom electrode, thus the metal will be directly deposited on the substrate without connecting to the metal layer that is on top of the photoresist as can be seen in figure 4.5. Since the material deposited on the substrate is supposed to be physically disconnected from anything touching the sacrificial layer, defects are less likely to be created when the photoresist gets stripped.

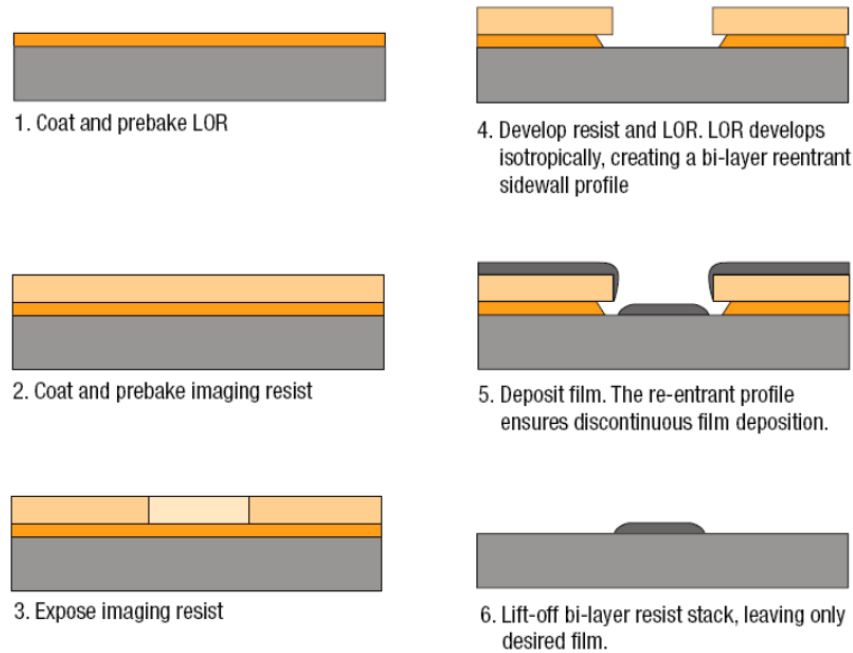
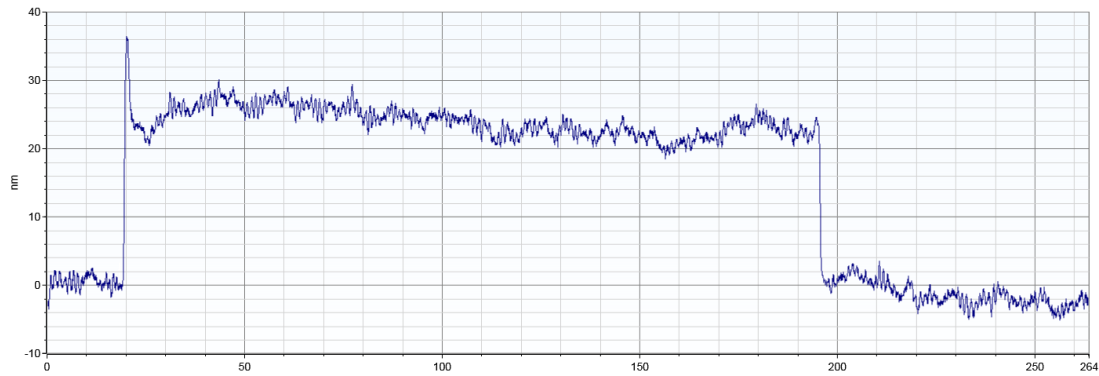


Figure 4: Graphical explanation of the liftoff process [9].

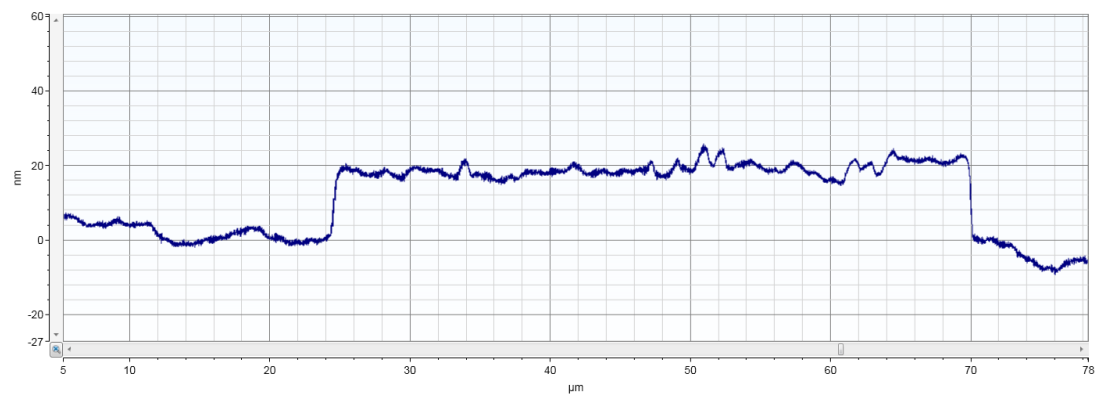
To model the pattern in the photoresist, we need to expose it using light. To do so, the MLA150 has been used [10]. This is a powerful machine that works either with wafers or chips. It allows you to print a design using a computer file (just like the one in figure 3) rather than having to create a physical chromium mask beforehand. Many parameters need to be tuned to get the best possible result. In this exposure, the 405 nanometers wavelength laser has been used coupled with a dose of 55 mJ.cm^{-2} and a defocus of -2.

The final lithography step is development. When the photoresist gets hit by the exposing light, the chemical bonds are affected and the location becomes more soluble in the developer. This chemical solution then helps to remove the exposed areas, leaving open the sacrificial layer according to the desired design. In the ANEMS group, we like to develop twice when a liftoff is performed. This allows for the LOR film to be slightly overexposed, leaving a larger gap under the top masking layer. This ensures that the metal does not come into contact with the LOR, further limiting the risk of defects appearing. A picture made with the microscope of one of the photoresist openings will be shown in figure 6a.

At first glance, any metal could be chosen to constitute the bottom electrode since we need a material capable of conducting electricity, but we also need it to be very resistant to solvents and very corrosive chemical solutions since some will be used in the future fabrication steps. We also need it to be as chemically stable as possible, as we do not want it to get easily oxidized. For these reasons, we used platinum as it fits very well these specifications. The only downside of this material is that its adherence is quite low, that is why we decided to use a 2 nanometers chromium (Cr) adhesion layer.



(a) Mechanical profilometer measurement of a 2 nm of Cr and 18 nm of Pt thin film made with EVA760. A fence of approximately 15 nm is detected on the left of the step. The actual thickness of the bottom electrode is also a bit off the 20 nm target.

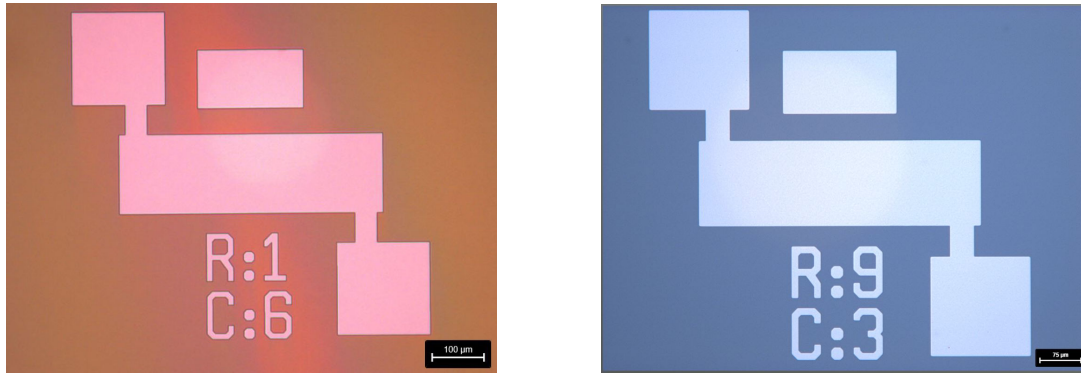


(b) Mechanical profilometer measurement of a 2 nm of Cr and 18 nm of Pt thin film made with LAB600H. No fence is to be seen and the actual thickness of the bottom electrode is very close to the 20 nm target.

Figure 5: Mechanical profilometer measurements comparison of (a) EVA760 and (b) LAB600H for the deposition of the Cr+Pt bottom electrode.

The 20 nanometers bottom electrode thin film was deposited using evaporation, in which the desired material is heated then evaporated on the wafer in a vacuum environment. The machine is made in a way that the working distance (distance from source to substrate) is crucial when it comes to film deposition homogeneity. This is why we wanted to confront the results obtained by using both of the available evaporation machines in CMi: EVA760 [11] and LAB600H [12]. The former should perform worse as the preferred working distance for liftoff is only 450 millimeters, which is less than half of the one in LAB600H (1010 millimeters). After the stripping of the resist, the test was to use a mechanical profilometer [13] to measure the step from the substrate to one of the deposited structures. The results obtained are visible in figure 5. The superiority of the Lab600H for this application is very clear: it delivers a film without fences whose thickness is impressively close to that desired.

The last step is to strip off the photoresist mask. To do so, the wafer is left overnight into a solvent bath. The solvent used in this case is the Remover 1165. It is crucial to make sure that the wafer is not directly facing up or part of the film might redeposit on the substrate. It



(a) Picture made with the microscope of the developed pattern of the bottom electrode in the photoresist.

(b) Picture made with the microscope of a structure's bottom electrode deposited by evaporation using the LAB600H machine.

Figure 6: Microscale picture of the bottom electrode photoresist mask and resulting deposition after liftoff of the bottom electrode.

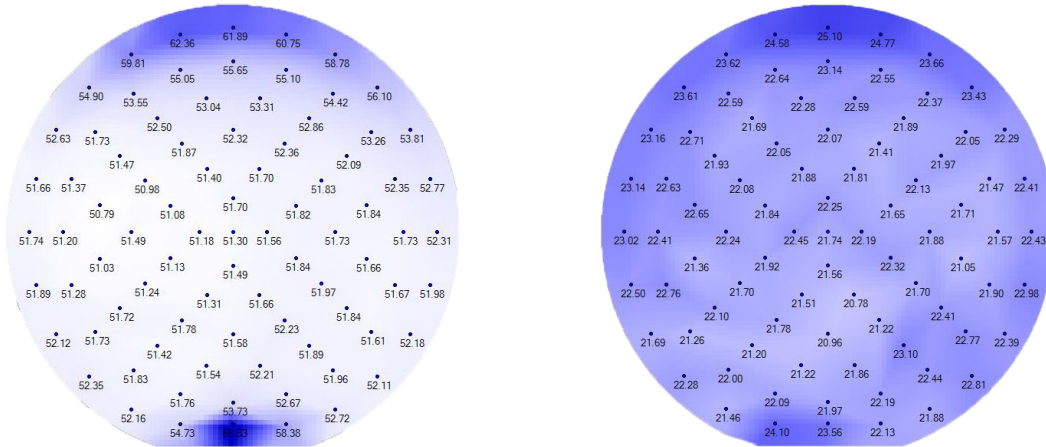
should be placed in a way that allows for the sacrificial layer to fly away. One of the bottom electrode after liftoff is shown in figure 6b.

2.3 Dielectric deposition and top electrode evaporation

The hafnium oxide and platinum top electrode films were deposited on the whole wafer in order to then be etched in the pattern that we need. To explore the impact of dielectric film thickness on the fabrication, we decided to process two distinct wafers with two diverse HfO_2 thicknesses: one with 25 nanometers and the other with 50 nanometers. The deposited HfO_2 thin-films thickness was measured using a thickness mapping system [14] whose results can be seen in figure 7.

The deposition of the hafnium oxide has been carried out by using the principle of Atomic Layer Deposition (ALD) in which we slowly grow a thin-film by alternating the use of two precursors gases that will sequentially react with the surface one at a time. To deposit hafnia, the first precursor is Tetrakis-(EthylMethylAmido)-hafnium (TEMAHf) which has to be at a temperature of 80°C and the second is Dihydrogen Monoxide (H_2O). It was processed using the CMi machine ALD BENEQ TFS200 [15] with the following parameters: 250 or 500 cycles (depending on the desired thickness) at a chamber temperature of 200°C and a 250 sscm nitrogen (N_2) environment.

As specified in section 1, flexoelectricity will create a curvature of the beam without the need for a shift in its neutral axis. This is the major difference with piezoelectricity and that is the reason why ideally, we want the bottom and top electrodes to be the same thickness. In a world where this is the case, no unwanted piezoelectric effect could affect the bending which simplifies the characterization measures of the flexoelectric coefficient. Even if this is much harder to achieve in reality, this is the reason why we decided to deposit the top electrode as a 2 nanometers Cr adhesion layer and an 18 nanometers Pt thin-film, just like on the bottom. To do so, the evaporation technique is used again. Since we're not doing liftoff here, the



(a) Thickness mapping of the targeted 50 nm thin-film of HfO_2 after ALD deposition.

(b) Thickness mapping of the targeted 25 nm thin-film of HfO_2 after ALD deposition. We are close to the resolution limit of the measuring machine.

Figure 7: HfO_2 thicknesses obtained by ALD deposition. Measurements were obtained by using the Filmetrics F54 thin-film mapper available in CMi [14]. The measured values on the edges can be a bit off target but it has no influence since it does not affect any structure.

quality of the deposition is not as critical as for the bottom electrode, which explains why we used EVA760 for this one. This is only because it is much more convenient due to the availability difficulties of the LAB600H, but we probably would have used the latter if that had been possible.

2.4 Top electrode patterning

Now that the wafers are entirely covered with the dielectric and top electrode thin-films, we need to pattern them according to our design. Obviously, we will have to etch through these layers but we need to operate photolithography first. As in section 2.2, this takes place as a photoresist coating, followed by exposure and to finish with the development of the exposed area. In the mentioned section, the goal was to liftoff so we wanted to open the sacrificial layer according to our pattern but now we will perform etching which means that the remaining photoresist is going to protect the film underneath it. Thus, the structures will be printed under the mask and not in its openings.

During the whole process flow, we had to make sure that the electrodes did not get shorted in any of the steps. This is crucial because it is the potential difference between them that will bend the dielectric due to flexoelectricity. We had to try several ways to process the top electrode patterning, to make sure no short-circuits appeared during this step. The change with the biggest impact on this shorting issue is the photoresist type. At first, a 700 nanometers AZ 10XT-07 coating was used to protect our layers but the electrodes were always shorted due to Pt redeposition, so we tried to change it to a 1 micrometer AZ ECI 3007 layer, and even without modifying the etching, we started to get much better results. For this reason, the 1 micrometer AZ ECI 3007 became our default photoresist coating when it came to etching.

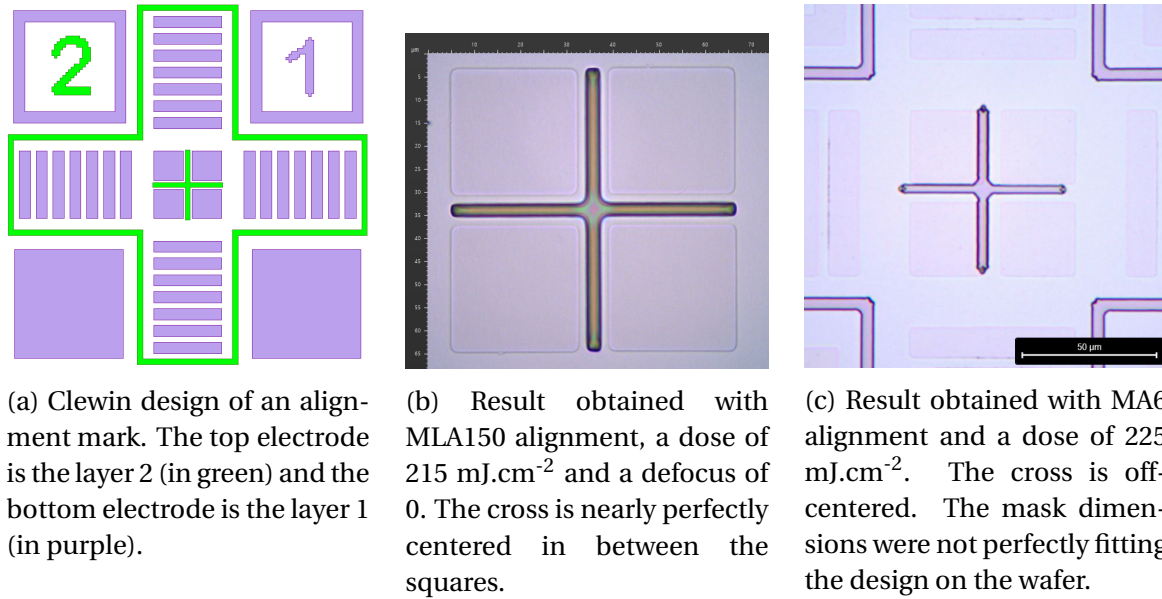


Figure 8: Comparison of the (a) alignment marks from the mask design software with the (b) MLA150 alignment and the (c) MA6 alignment. The cross from the top electrode should be centered in the 4 squares design.

To perform the photoresist exposition, two machines can be used. The first one is MLA150 [10] — the same than the one that we used to expose the bottom electrode, and the second is the MA6 [16]. To use the latter, a chromium mask has to be ordered and etched beforehand. It is good if you have to replicate a design multiple times but shows weaknesses in the alignment. Alignment is a fundamental part when it comes to exposing photoresist on top of an already patterned structure. Indeed, we need to make sure both motives are aligned according to the general layout of our design. We cannot afford to have overlapping electrodes or short-circuits will appear. For this reason, alignment marks were patterned in the first layer. They will allow us to give some reference points to the exposing machine so it can adjust the position of the design to fit the bottom electrode. Our alignment marks pattern can be seen in figure 8. The MA6 alignment is weaker than the one from MLA150: firstly because it is done manually using a joystick and a microscope, which is less precise than a computer; secondly because if there is a size mismatch between the mask and the bottom electrode design — even of a few hundreds of nanometers — it becomes impossible to perfectly superimpose the mask in the center of each alignment marks. It still has some advantages such as a great speed of use and a short exposure time compared to the MLA150, but this project is not about quantity but quality so I would advise using the MLA150 — with a dose of 215 mJ.cm^{-2} and a defocus of 0 — to make sure that both the alignment and exposure are as good as possible.

The etching of the films is done in two steps: a dry and a wet etching. In our case, wet etching is appreciated because the etched material is chemically reacting with the liquid which limits the possibility of residues redepositing on the substrate, in contrary to the dry etching process.

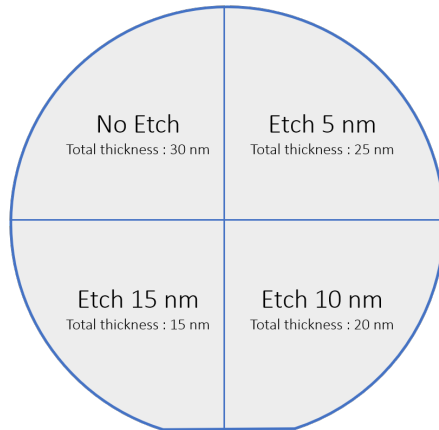


Figure 9: Representative diagram of the four different thicknesses quarters.

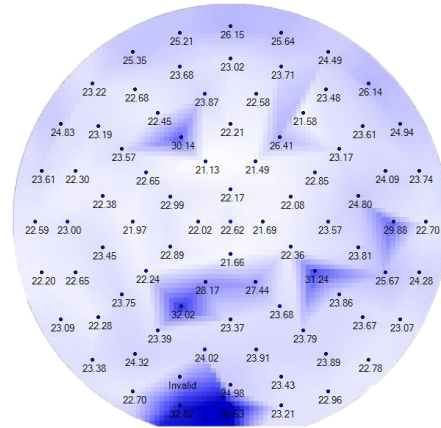


Figure 10: Thin-film mapper [14] measurements of the HfO₂ thickness after the ion beam etching of the Pt and Cr layers.

As explained before, platinum is an inert material which makes it one of the most difficult metals to pattern. For this reason, wet etching is not really suited and the common way to etch Pt is through ion beam etching. This process working principle is that ions are extracted from a source, then they get accelerated and directed so they form an energetic beam of ions that can etch any material by pure physical sputtering. According to this, we decided to use the IBE350 machine available in CMi [17]. This machine is fairly easy to operate, one can choose four different power settings, tune the substrate fixture tilt angle and the etching time. We were always using the low power setting since the etch rates of our materials are in the order of our films' thicknesses. The other parameters will be discussed later in this section.

Once the top electrode is removed, the hafnia is exposed and it can be etched. On the CMi website, the only bath that is referenced as a HfO₂ wet etchant is the buffered oxide etch also known as BHF. It is a 7:1 volume ratio of NH₄F 40% to HF 50%. We decided to try it even if the etch rate is only 1.5 nm.min⁻¹. We had to dip it for a very long time and the results were pretty awful. The structures started to fly away and the substrate has been completely damaged by the acid. Another solution had to be sought. We found in Kaitlin Howell's thesis that she performed some etching test on this material and it resulted that hafnium oxide is etched at a rate of more than 65 nm.min⁻¹ in a 1:4 volume ratio of HF 49% to H₂O solution [1]. We came to the conclusion that we would use it for this part of the process, so we decided to dip the wafer in the bath for one minute to remove the dielectric layer. It could be reduced for the 25 nanometers HfO₂ wafers, but the hydrofluoric acid (HF) won't damage any structure in such a short time.

At the start of this project, we wanted to maximize the variety of actuators that could be fabricated on a wafer by depositing a 30 nanometers top electrode that would be etched in quarters of diverse thicknesses (see figure 9). This would allow various adjustments of the neutral axis, but it lengthened the fabrication since each quarter had to be etched separately, and having diverse thicknesses can make it hard to process the wafer. Indeed, since the current steps are done at a wafer level we had to etch in a way that would remove the thickest

quarter of the Pt film but without getting to the bottom electrode in the thinnest one since the ion beam etching (IBE) will also etch the HfO_2 . Even if we abandoned the quarters' idea, the wafer that we processed in this way gave us good information about the etching. In the first etching that we did, we calculated the exact time that would remove the 30 nanometers quarter to make sure we do not over etch the thinnest one. After putting it in the HF bath, we saw that the hafnium oxide in the top left quarter (the thickest one) was not going away. We concluded that this was probably because the chromium adhesion layer had not completely disappeared during the ion beam etching. According to CMi, Cr acts like a mask in the hydrofluoric acid solution. To overcome this, we decided to come back to the uniform 20 nanometers top electrode and to make sure we start to etch through the dielectric film when using IBE to pattern the Pt thin-film. We can use the thin-film mapper [14] again to make sure that the platinum and chromium are all gone from the surface (as in figure 10). Another good way to know if we landed in the hafnia is to use a multimeter to measure the surface resistivity. If the measured value is "overload" (OL) then it is HfO_2 , if not then we did not reach it yet.

The last parameter that has to be addressed is the substrate fixture tilt angle. It can be set in a range from $+90^\circ$ to -70° . In this machine, the larger the angle, the less redeposition there will be, but the etching will become non-uniform and will begin to be slower in the middle. Following an advice, we tried the -10° , -20° , and -30° angles on chunks of a cleaved wafer. To determine the best setting, we used the TS150 probe station in CMi [18] to measure the resistivity of several structures on each of these chunks. The best number of working structures over the number of structures tested ratio was obtained by the -30° angle with around two-thirds of non-shortened devices.

In conclusion of all these tests, our final process to etch the top electrode is to first put the substrate in IBE350 in low power setting for 2 minutes (1m10s if working with the 25 nm HfO_2 thin-film) at a -30° angle and then to dip it for one minute in the hydrofluoric acid solution.



(a) Top electrode photolithography done on a wafer with 50 nm of HfO_2 . The alignment and exposure were performed with MLA150.

(b) Example of a structure obtained after the top electrode patterning.

Figure 11: Microscope pictures made after the main steps of the electrode patterning.

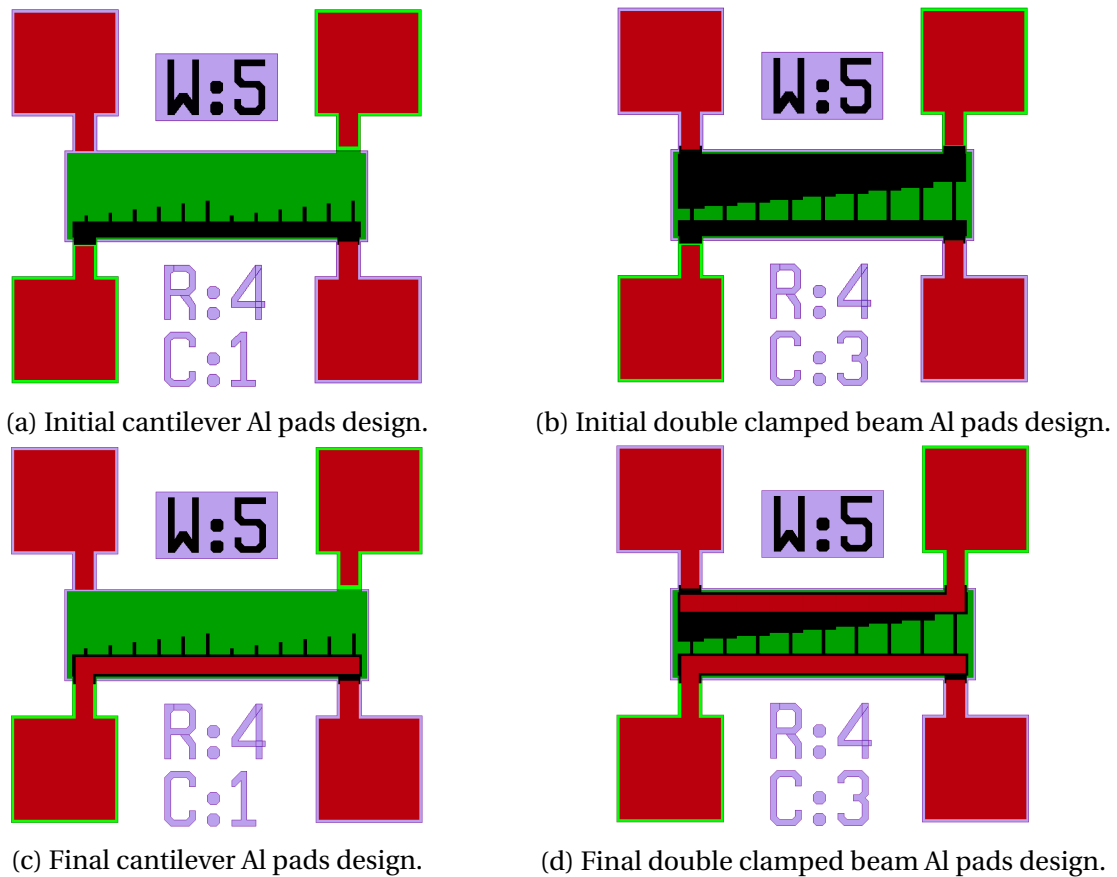


Figure 12: Clewin mask design of a structure with the various designs of Al pads (in red).

2.5 Al pads liftoff and dicing

The deposition of the aluminum pads is very similar to the one from the lower electrode. The sacrificial layer composition and thickness stay the same: a 1.1 micrometers film of AZ 1512 stacked onto a 480 nanometers deposition of LOR. The photolithography step is also done in the exact same way as in section 2.2 — we still use the MLA150 without changing any parameter except that the design has to be aligned. The liftoff step was operated in the same way as well, only changing the metal to a 500 nanometers aluminum thin-film evaporated using EVA760 since the homogeneity of this deposition is not critical.

To improve the conduction of the top electrode, we changed the initial design. The idea is to take advantage of the 4 times higher conductivity of aluminum compared to platinum by covering the Pt electrodes with Al as much as possible. The initial and final designs are illustrated in figure 12.

Now that all of the wafer-level fabrication steps are done, it can be diced in chips. To do so, we cover the whole wafer with a 1-micrometer coating of AZ ECI 3007 to protect the devices. Dicing marks were patterned during the bottom electrode layer deposition in the corner of each chip to make it easier to know where to cut. At the end of this step, each wafer gives 24 chips that can be processed one at a time. This is very helpful in our case since we can now perform our tests without the need to restart the whole process each time we face an issue.

2.6 Actuators patterning

This step is certainly one of the most challenging. Many things can go wrong and the reason why it does is not always obvious. Very often, the structures got shorted at the end of this part of the process flow. We will first speak about the lithography and then the etching will be discussed.

Two machines can be used to create the protective layer that will allow us to pattern and etch the actuators: the MLA150 [10] and the EBPG-5000+ [20]. We already know very well the first machine and the second one is an electron beam (e-beam) lithography system. Electronic lithography is based on the same overall principle as photolithography but the light is replaced by an electron beam. Just like with photons, when the electrons get to touch the resist coated surface, they change the properties of this electron-sensitive film which makes it soluble in the developing solution. This technology is used to print very small designs with a resolution up to a nanometer as it allows to go beyond the limits imposed by the diffraction of light. The first step is to coat the chip with the electron-sensitive resist. In this case, we chose to go with 600 nanometers of CSAR 62 due to its good dry etch selectivity. Now that we work with chips, the resist deposition has to be done manually with a manual coater. Then the chip is placed on the holder. This part of the procedure for using the machine is quite long and delicate since the holders of this tool are very fragile and complex systems on which the alignment is done manually. These holders can carry up to two chips at a time. The actual exposure — the fastest part of the procedure — needs the user to enter a value for the dose parameter. This is very application-specific and the typical doses for CSAR 62 are in a range from 160 to 400 $\mu\text{C}\cdot\text{cm}^{-2}$ so a dose test was performed on a wafer chunk. It revealed that the needed dose parameter is 250 $\mu\text{C}\cdot\text{cm}^{-2}$. When the dose is lower than this value, we have resist residues remaining in the opening and when the dose is bigger than this value, the actuators shape gets thinned. These results can be seen in figure 13.

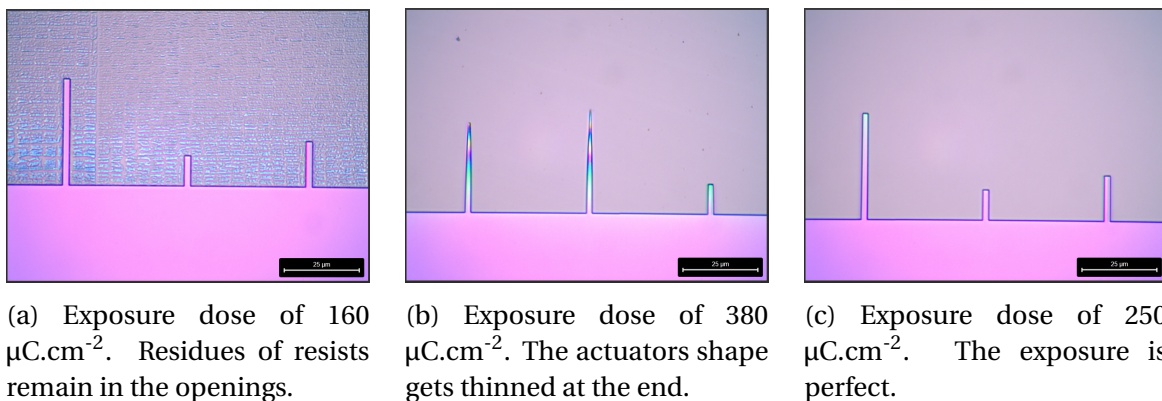


Figure 13: Results obtained with the e-beam dose test performed on a wafer chunk.

MLA150 is also very good to work with chips. We only need to coat it with a 1-micrometer film of AZ ECI 3007 and it is ready to be exposed in the machine. No need for a dose test since we already used the machine to pattern the top electrode, so we know that 215 $\text{mJ}\cdot\text{cm}^{-2}$ and a defocus of 0 is going to work with the platinum underneath the photoresist layer. The figure 14 aims to compare the lithography obtained with MLA150 to the one with e-beam.

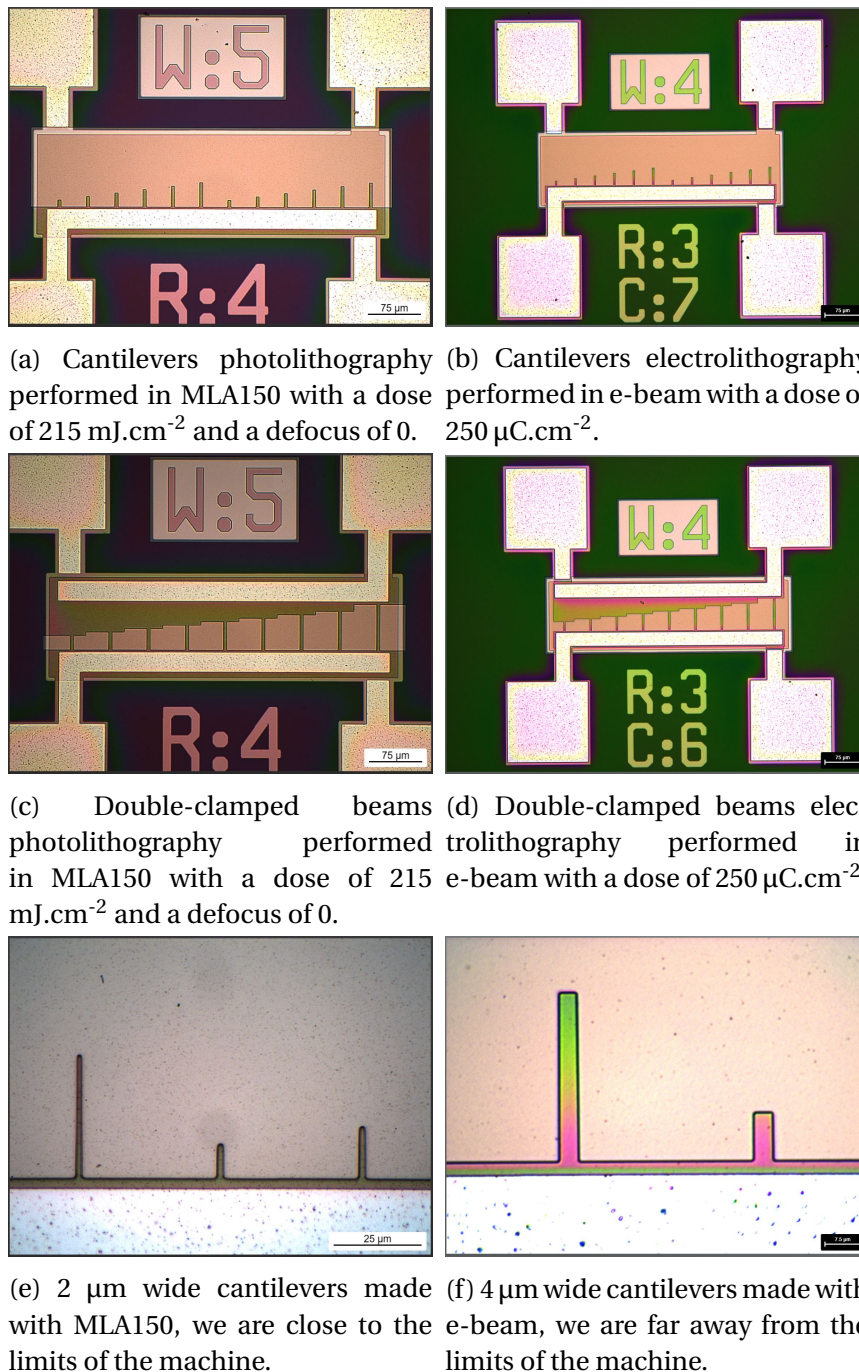
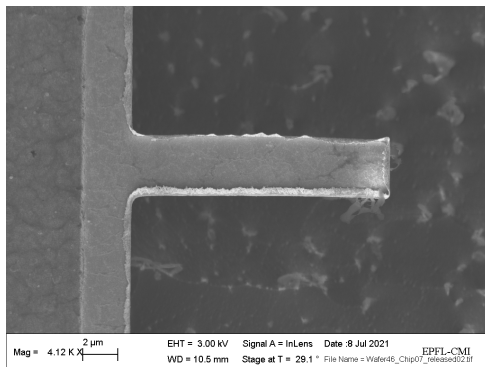


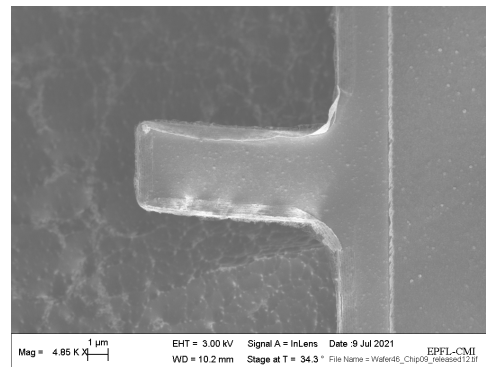
Figure 14: Comparison of the photolithography (MLA150) with the e-beam lithography (e-beam). The latter allows better precision at the cost of increased complexity and overall processing time.

Sadly, our actuators' size is in between the two resolution scales of the machines. The design is very big from the e-beam point of view but very small from the MLA150 point of view where we play with the resolution limit. In theory, both could be used, the photolithography has the advantage of being fast and easy to operate compared to electroplithography which allows for more precise patterning of the devices. The conclusion that we drew about this dilemma is that the MLA150 is probably good enough for this application but we still wanted to try both of the options coupled with the etching.

We can now dive into the etching. This part is certainly the most delicate of the whole process flow since we need to make sure that it will not short the whole structure. The first thing we tried was masking the chip with the 600 nanometers of CSAR 62 and etching through the whole film stack until silicon using the IBE350. The idea was to perform the etching in a known way with the best mask precision we could get. Unfortunately, 4 minutes and 45 seconds in the machine (on low power setting at an angle of -20°) resulted in a burnt resist and a chip with only one working structure, all the others having been shorted out. At this time, we thought the machine could be trusted because it was the best solution we found to etch the top electrode so we questioned the resist choice. Maybe what happened with AZ 1512 in section 2.4 was happening again with the CSAR 62, so we decided to try to use the AZ ECI 3007 again. This time we divided the etching into 5 one minute steps to reduce the chances of the photoresist burning and increased the angle to -30° . Again, the structures were mostly shorted so we decided to take a look in a scanning electron microscope (SEM) [21], the pictures can be seen in figure 15. High fences are visible on both the electron beam and MLA150 shaped actuators, they probably are the reason for the shorting issue, supporting the idea that the IBE350 is not the proper tool for this job.



(a) Cantilever obtained through electroplithography.



(b) Cantilever obtained through photolithography.

Figure 15: Scanning electron microscope (SEM) pictures of the actuators obtained with both the lithography techniques. Fences are present in both chips.

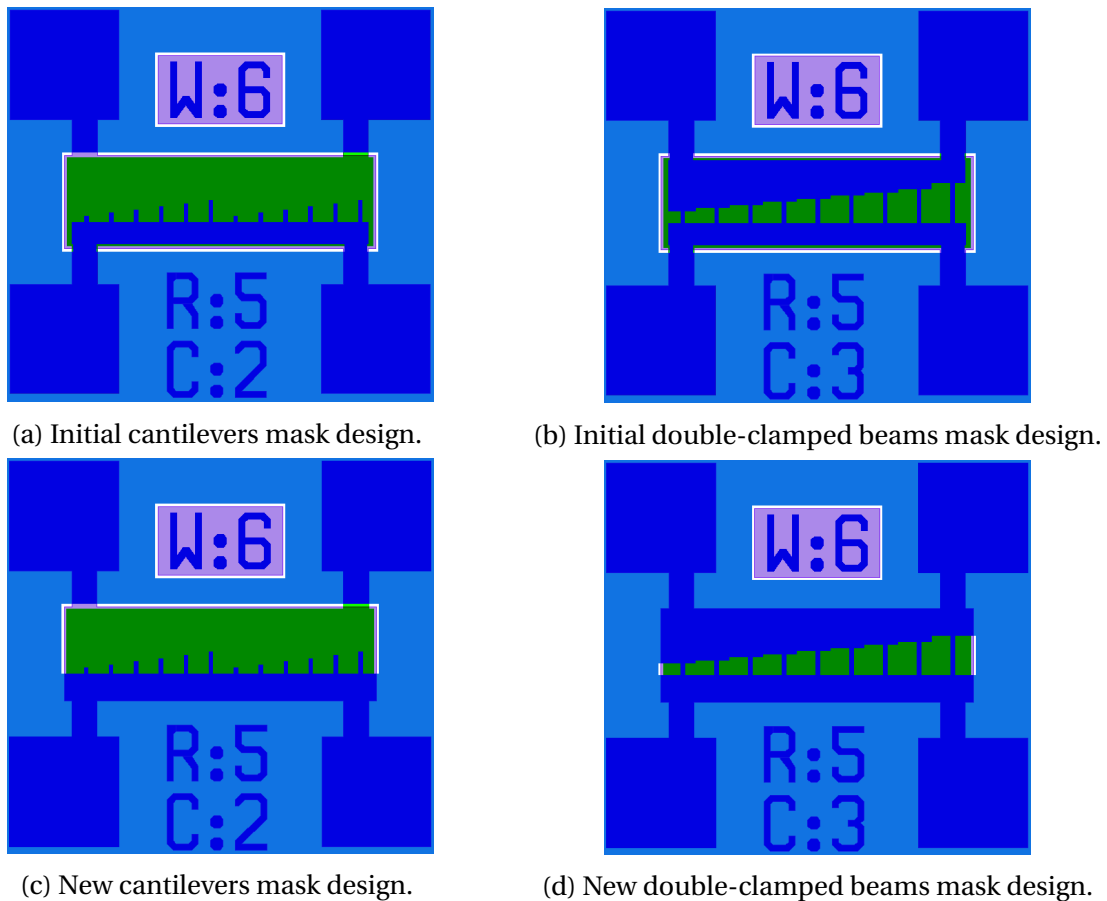


Figure 16: Comparison between the initial and the new design for the mask modeling the actuators. The resist remaining after development is shown in shades of blue, the other colors represent the areas that are free to be etched. The Al pads were hidden for clarity purpose.

Despite these bad results, we continued to search for a promising way to perform this etching. We decided to prepare a new chip in MLA with a slightly different design. The idea behind it was to reduce the etching area as much as possible to limit the places where short-circuits could appear. The previous and new designs are shown in figure 16. Along with this change, we also tried to use the STS dry etching machine available in CMi [22] to pattern the actuators. To do so, we used the recipe Pt_etch because we knew that it would remove the platinum and the HfO_2 , but we did not know at which rate exactly so we let the chip for 6 minutes of etching in the tool to make sure all of the three layers were gone and that we correctly landed in the silicon. This time, the top and bottom electrodes of many structures were still electrically isolated from each other, leading us to believe that the STS is a much more suited tool for this part of the process. To make sure, we used the SEM again after the actuators release to take the pictures that can be seen in figure 18. No fences appeared using this dry etching tool which reinforces the idea that they are at the origin of the short-circuits. We also see that the MLA150 loses a bit of precision but the actuators obtained are sufficiently well patterned for the application.

2.7 Actuators release

Now that the actuators are patterned and laying on the silicon substrate, we can release them. To do so, we just need to take advantage of the Si isotropic etching properties of the sulfur hexafluoride (SF_6) gas. This last step is performed in the AMS 200 machine available in CMi [19]. On the website, they say that the recipe will etch around 4 micrometers in vertical and 2 micrometers in lateral, but it depends on the design. To make sure we don't have any kind of over-etching, we chain several etching steps of 1 minute until the beams are released. Usually, they get free after 4 steps, that is to say 4 minutes of etching in total.

We can use the microscope to know if the release is over. The trick is to look for a bending of the beams by progressively moving the focus up or down. If the focus moves along the beam, then it means that the height of the actuator changes due to the curvature (phenomenon illustrated in figure 17). It is induced by the stress in the films but it is not an issue, it just needs to be taken into account when doing the calculations and measurements.

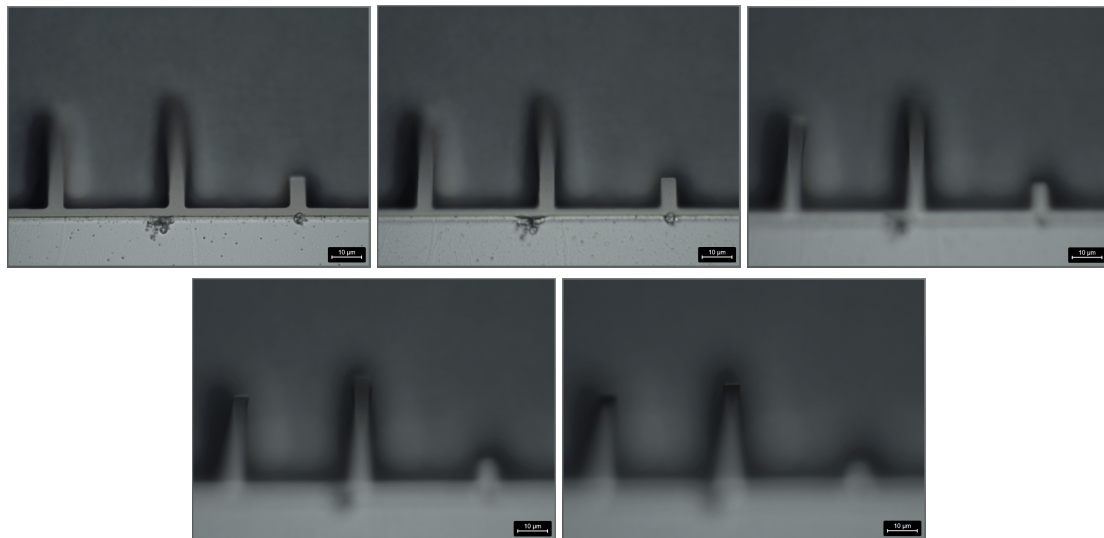


Figure 17: Microscope pictures of the bending of some beams. The focus is going up from a picture to the other, meaning the beams bend upward.

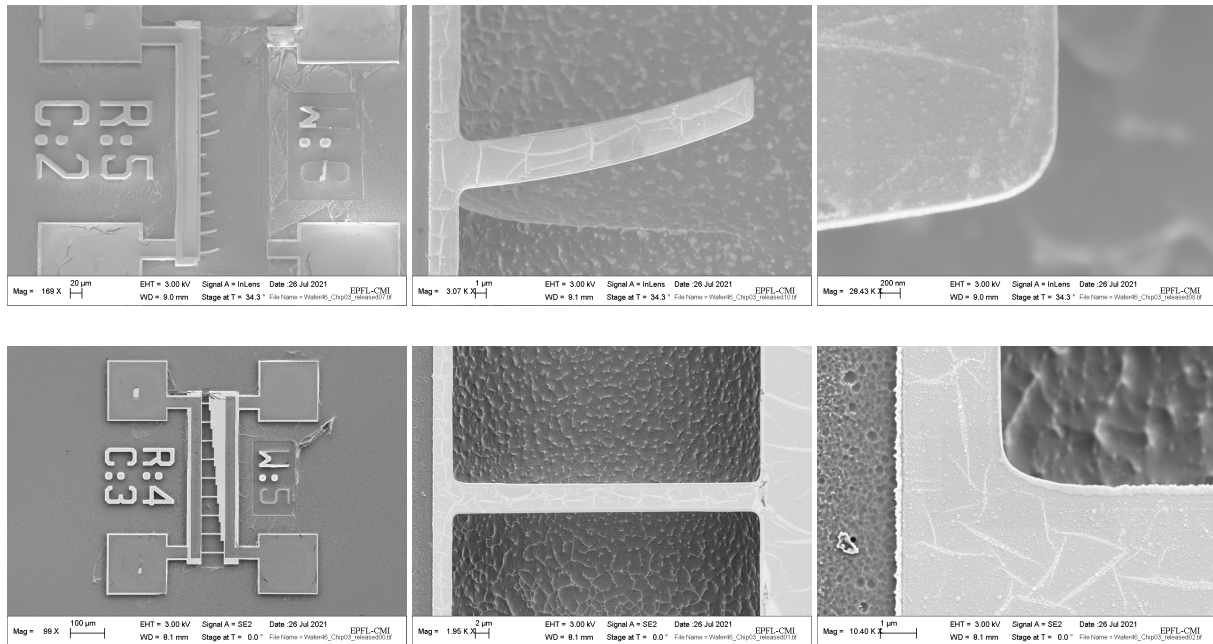


Figure 18: Scanning electron microscope (SEM) pictures of the final result. These are the devices obtained with photolithography followed by STS dry etching. No fences are to be seen but the surface purity could be improved.

2.8 Measurements

Every hour spent in the cleanroom trying to optimize every part of the manufacturing process was aimed at this final measurement. Through our work, we have been able to create non-shortened flexoelectrically actuated devices based on hafnium oxide. The figure 19 is the proof that this final process flow (which can be found at the end of this document) is suited to be the base for the HfO_2 flexoelectricity coefficient characterization project.

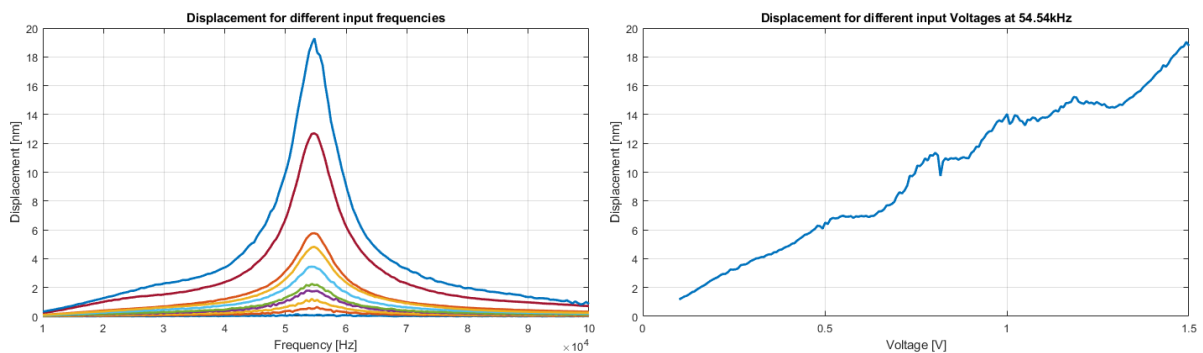


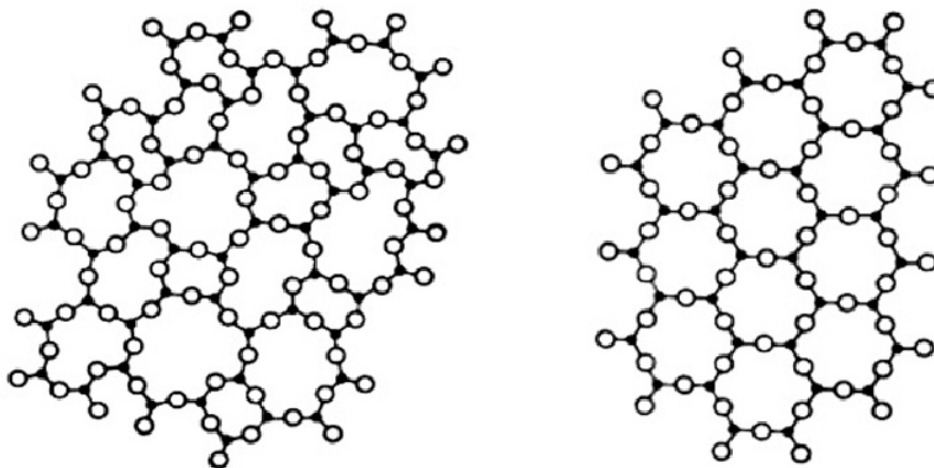
Figure 19: Measurements performed with the Laser Doppler Vibrometer from the ANEMS laboratory on a cantilever patterned with MLA150 [10] and etched by the STS machine [22].

3 HfO₂ crystallization

In this second part of the thesis, the crystallization of the wafers will be studied. We need to make sure that we are able to do it correctly as crystalline hafnium oxide flexoelectricity will be characterized in the future of the main project. This part is a first glance into the crystallization process of our devices, the goal is to get a better understanding of what we need and how the annealing operation is done.

3.1 What is crystallization ?

In microfabrication, most of the thin-film standard deposition processes will grow an amorphous (or non-crystalline) layer which means that in the deposited material, atoms are not ordered in the medium to long range. This state of matter is fundamentally opposed to crystals, where atoms form what's called a crystal lattice — a highly ordered microscopic structure — that gets replicated all along the material. Crystallization is the process by which the arrangement of atoms in an amorphous film gets reorganized into a highly ordered crystal lattice, thus forming a crystalline layer. This is obtained through annealing, which is a heat treatment consisting of heating the material above its recrystallization temperature — from which the atoms constituting it start to reorganize — for a certain time before cooling it down. The temperature at which the film gets heated plays an essential role in the obtained results. Indeed, in crystallography, there are seven different crystal systems, each with a different arrangement that will influence the characteristics of the material.



(a) Example of atoms disposition in an amorphous solid.

(b) Example of atoms disposition in a crystal.

Figure 20: Comparison of the (a) amorphous and (b) crystalline states of an arbitrary material [23]. Both arrangements appear organized in the short range, but in medium to long range the placement of the atoms in the amorphous film looks messy.

3.2 Crystallization process

To build the annealing process parameters, we need to choose the type of crystallization that we are willing to obtain. The atoms in hafnium oxide can rearrange in three distinct phases: monoclinic (m-phase), tetragonal (t-phase), and orthorhombic (o-phase). The latter is an asymmetric arrangement, which causes the HfO_2 film to show piezoelectric behavior. It is obtained by annealing the dielectric film to the tetragonal phase followed by a cooling with a capping layer [24]. However, as explained in section 2.3 this is not a property of HfO_2 that we want because it can influence our measurements. Fortunately, the most stable at ambient conditions is the monoclinic phase, which is the one that we will aim for.

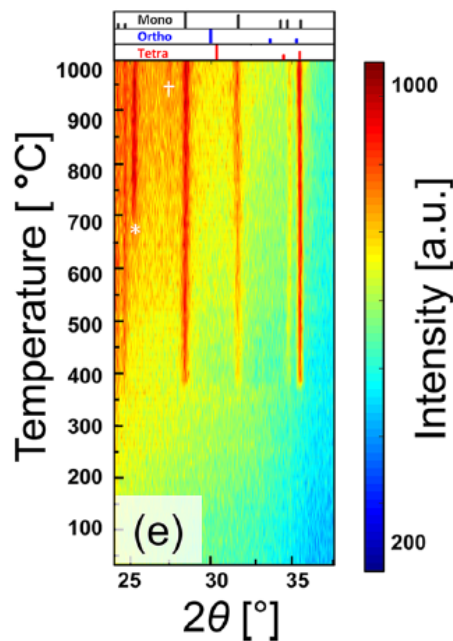


Figure 21: High temperature in situ x-ray diffraction (HTXRD) of 30 nm thick HfO_2 [25].

The figure 21 is a x-ray diffraction (XRD) measurement taken from a crystallographic study on HfO_2 -based 30 nanometers thin-films [25]. It was performed during the annealing in order to be able to build this heat map that gives very good information about the hafnium oxide crystallization kinetics. Based on this, we will anneal both 25 and 50 nanometers HfO_2 films caged between two layers composed of 2 nanometers Cr and 18 nanometers Pt, just like the electrodes in our structures.

In the aforementioned article, the substrate was heated up and cooled down at a rate of $2^\circ\text{C}\cdot\text{min}^{-1}$. This was so slow because the XRD measurements were performed during the annealing. This is not our case so we decided to heat up our samples at a rate of $20^\circ\text{C}\cdot\text{min}^{-1}$ and cool them down as fast as possible using convection. We will also replicate the N_2 environment that was used in the crystallographic study. Since we arbitrarily chose to anneal our samples for 1 hour at 500°C , 600°C , and 700°C for this test, we will use the Neytech Qex furnace [27] available in CMi because it is suited to each of these parameters.

3.3 Crystallization results

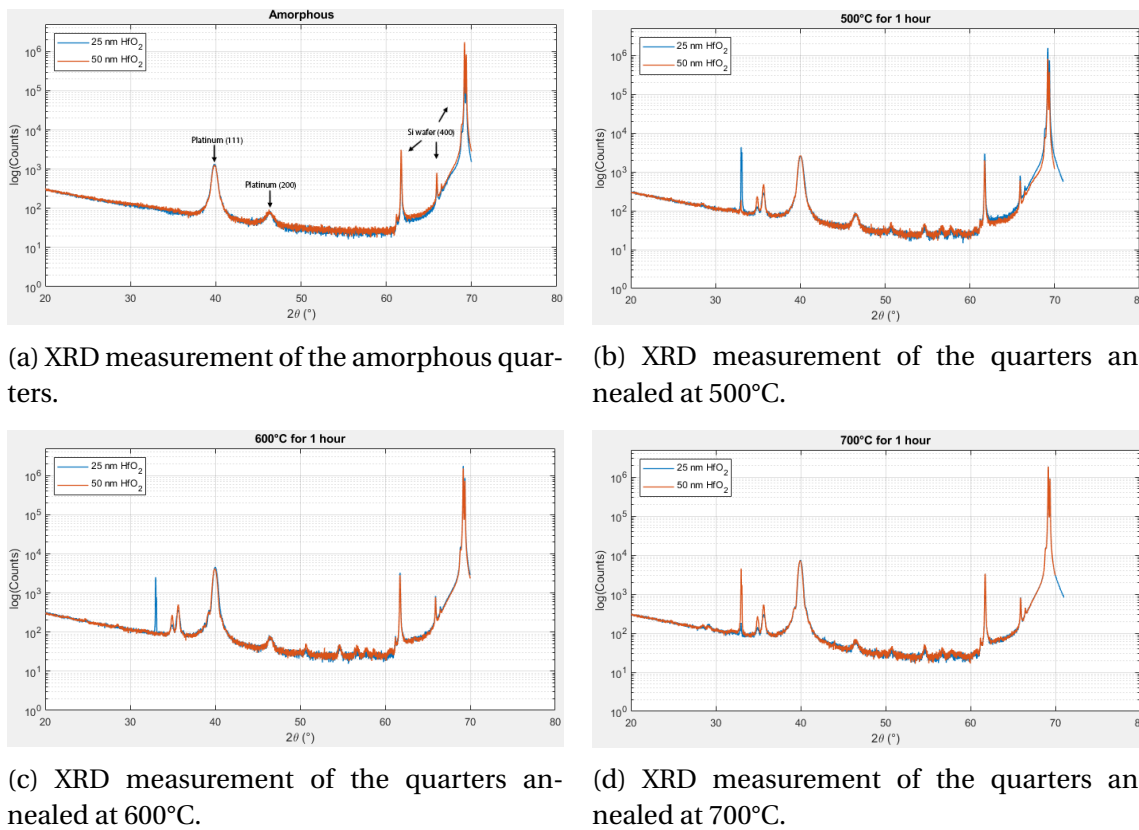


Figure 22: X-ray diffraction (XRD) measurements performed on the quarters from our crystallization tests. For each annealing temperature, the intensity curves of the 25 nm and the 50 nm wafers are plotted together.

Each quarter having been individually annealed, we performed an XRD measurement to obtain the composition of each quarter. The results are plotted in figure 22. To start the analysis, we wanted to get a better understanding of the origin of each peak. We started with the amorphous situation since it shares all of its peaks with the other cases. The first two peaks in 40° and 46.5° are due to the platinum and the three remaining in 62°, 66°, and 69° are originated from the silicon substrate. It is totally normal to have two Pt peaks because they represent different planes, but for the Si, we should see a unique peak in 69°. All three of them account for the same plane and this can be explained by the contamination of the XRD spectrum, meaning that the x-ray coming from the source is not strictly monochromatic [28]. Since we have more than one wavelength, Bragg's law gets verified for more than a single angle (or peak), which explains why the Si lattice reflects the ray for several incident angles.

Now that we understand the origins of the shared peaks, let's dive into the ones appearing after the annealing process. This concerns the peaks at 33°, 34.9°, and 35.6°. The leftmost is due to the forbidden reflection of silicon and it can appear or disappear from one measurement to another. Due to this randomness, we chose not to worry about it but its origins are still very unclear to me due to my lack of knowledge in material science, so it might be worth

looking into it in more depth. The two remaining peaks are the ones that we really care about: they are completely missing from the amorphous measurements but are always present in those of the annealed quarters, which supports the fact that they account for the hafnium oxide crystallization. We know by looking at the top of figure 21 that peaks around 35° are to be expected in the monoclinic and tetragonal phases, so it is difficult to draw conclusions without other peaks in the values where they should be more separated. As explained in the previous section, cooling down the HfO_2 film from the tetragonal phase with a capping layer should lead to the orthorhombic phase. This would mean that the two peaks close to 35° are describing the m-phase since the o-phase has lower angle value reflections.

We can reasonably think that the two peaks that appeared after the annealing are the same as the peaks located furthest to the right in figure 21, reinforcing the idea that we are in the monoclinic phase. In fact, they are very similar both in their positions and in their relative intensity since the left peak is a bit lower than the right one. The lingering question is: why don't we have peaks around 24° and 30° ? A likely answer to this lies in the differences in the settings we have chosen. I contacted one of the editors of the article from which figure 21 was taken to ask her opinion. She replied to me that in their field, they usually avoid the HfO_2 monoclinic phase so they perform a quench cooling by cooling the sample down as fast as possible. She advised to slowly cool the sample and to reduce the holding time of the annealing temperature to 15 minutes or even less.

Another important point to address is the annealing temperature limit. In both the 25 nanometers and 50 nanometers wafers, the quarter heated up to 700°C showed some holes in the top platinum film. This never happened in any other quarter and it could be due to many different things such as thermal expansion, bad film adhesion, microcracks... Even if the origins of these impurities are unclear, this tells us that the annealing step should take place at a lower temperature than 700°C .

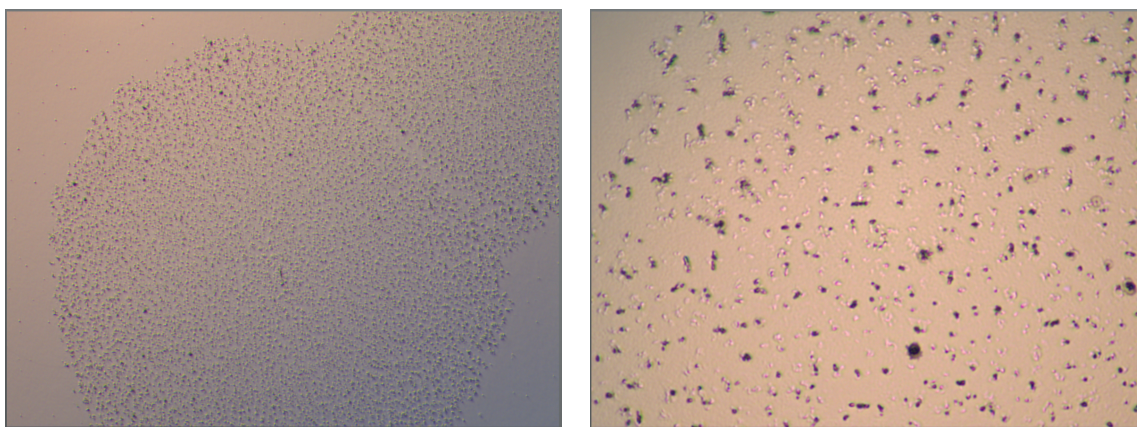


Figure 23: Formation of impurities in the upper Pt film after annealing at 700°C . Unfortunately, no scale bar is visible but the main goal is to illustrate this phenomenon.

4 Conclusion

The main objective of this project was to perform and optimize as many steps of the HfO₂-based actuators fabrication process as possible. Obviously, this is very time and money consuming since a single issue can force us to restart the whole procedure but we managed to squeeze a solid and fairly reliable process flow out of these tests (which can be found at the end of this report). We have been able to go through every step and even finish some devices that have proven to be able to be properly electrically set in motion.

It is always very challenging to fabricate nanoelectromechanical systems (NEMS) because of the many problems that can appear. One has to be very methodical, each step having its specificity. It also takes a good amount of precision because over-etching is quick to happen with such thin layers. Finally, you certainly need a bit of luck to link all of these steps together correctly. Fences have a huge impact on nanostructures and short circuits are easily created because the physical separation between the electrodes is on the order of a few tens of nanometers. These have to be avoided at all costs, but they also are inevitable. Remember that they are independent of each other and that it only takes a few structures that work well to get results.

Crystallization tests were also carried out since it will be necessary to control this phenomenon for the main project aimed at characterizing the flexoelectric coefficient of the various forms of hafnium oxide. This was a first step for us in this field and we managed to get a better understanding of it. The annealing procedure needs to be adjusted to best suit the desired results, some changes such as a decrease in the holding time and a slower cooling of the sample were discussed as future possibilities.

I hope this thesis will form a good starting point for the main project. This topic has been very stimulating to work on and I wish good luck to everyone who will have the opportunity to contribute to it.

References

- [1] HOWELL, Kaitlin Marie. Dielectric Actuation Techniques at the Nanoscale: Piezoelectricity and Flexoelectricity. *EPFL*, 2019.
- [2] History of MEMS.
https://nanohub.org/resources/26535/download/App_Intro_PK10_PG.pdf
- [3] ZUBKO, Pavlo and CATALAN, Gustau and TAGANTSEV, Alexander K. Flexoelectric Effect in Solids. *Annual Review of Materials Research*, 43:387-421, 2013.
- [4] BO Wang, YIJIA Gu, SHUJUN Zhang, LONG-QING Chen. Flexoelectricity in solids: Progress, challenges, and perspectives. *Progress in Materials Science*, 106:100570,2019.
- [5] BHASKAR, U., BANERJEE, N., ABDOLLAHI, A. et al. A flexoelectric microelectromechanical system on silicon. *Nature Nanotech*, 11:263–266, 2016.
- [6] QIAN Deng, MEJDI Kammoun, ALPER Erturk, PRADEEP Sharma. Nanoscale flexoelectric energy harvesting. *International Journal of Solids and Structures*, 51:3218-3225, 2014.
- [7] KWON S. R., HUANG W. B., ZHANG S. J., YUAN F. G. and JIANG X. N. Flexoelectric sensing using a multilayered barium strontium titanate structure. *Smart Materials and Structures*, 22:115017, 2013.
- [8] NEVELING, Deon. (2015). Re: "What is the difference between top down and bottom up methods for creating nano-structures?". Retrieved from:
<https://www.researchgate.net/post/What-is-the-difference-between-top-down-and-bottom-up-methods-for-creating-nano-structures/54ad3ce1cf57d73b448b46a8/citation/download>
- [9] LOR20B Ltoff Resist - Standard Operating Procedure.
https://engineering.tufts.edu/microfab/documents/SOP_Liftoff-LOR.pdf
- [10] CMi Machine - Heidelberg Instruments MLA150.
<https://www.epfl.ch/research/facilities/cmi/equipment/photolithography/heidelberg-instruments-mla150/>
- [11] CMi Machine - Alliance-Concept EVA 760.
<https://www.epfl.ch/research/facilities/cmi/equipment/thin-films/alliance-concept-eva-760/>
- [12] CMi Machine - Leybold Optics LAB 600H.
<https://www.epfl.ch/research/facilities/cmi/equipment/thin-films/leybold-optics-lab-600h/>
- [13] CMi Machine - Bruker Dektak XT.
<https://www.epfl.ch/research/facilities/cmi/equipment/metrology/bruker-dektak-xt/>
- [14] CMi Machine - Filmetrics F54.
<https://www.epfl.ch/research/facilities/cmi/equipment/metrology/filmetrics-f54/>

- [15] CMi Machine - ATOMIC LAYER DEPOSITION BENEQ TFS200 (ALD 1).
<https://www.epfl.ch/research/facilities/cmi/equipment/thin-films/atomic-layer-deposition-beneq-tfs200-ald-1/>
- [16] CMi Machine - Süss MA6/BA6.
<https://www.epfl.ch/research/facilities/cmi/equipment/photolithography/suss-ma6-ba6/>
- [17] CMi Machine - Veeco Nexus IBE350.
<https://www.epfl.ch/research/facilities/cmi/equipment/etching/veeco-nexus-ibe350/>
- [18] CMi Machine - MPI TS150 Prober Station.
https://www.epfl.ch/research/facilities/cmi/equipment/metrology/mpi_ts150/
- [19] CMi Machine - Alcatel AMS 200 SE.
<https://www.epfl.ch/research/facilities/cmi/equipment/etching/ams200/>
- [20] CMi Machine - Raith EBPG5000+, electron beam lithography system.
<https://www.epfl.ch/research/facilities/cmi/equipment/ebeam-lithography/raith-ebpg5000/>
- [21] CMi Machine - Zeiss LEO 1550.
<https://www.epfl.ch/research/facilities/cmi/equipment/metrology/zeiss-leo-1550/>
- [22] CMi Machine - STS Multiplex ICP.
<https://www.epfl.ch/research/facilities/cmi/equipment/etching/sts-multiplex-icp/>
- [23] ÇELIKBILEK M., ERSUNDU A. E. and AYDIN S. Crystallization Kinetics of Amorphous Materials. *Istanbul Technical University*, 2012.
- [24] ELISEI Andrea. Rapport de Projet de Semestre: High-K Dielectric NEMS. *EPFL*, 2020.
- [25] HSAIN H. Alex, LEE Younghwan, PARSONS Gregory and JONES L. Jacob. Compositional dependence of crystallization temperatures and phase evolution in hafnia-zirconia ($\text{Hf}_x\text{Zr}_{1-x}\text{O}_2$) thin films. *Applied Physics Letters*, 116:192901, 2020.
- [26] HO M.-Y., GONG H., WILK G. D., BUSCH B. W., GREEN M. L., VOYLES P. M., MULLER D. A., BUDE M., LIN W. H., SEE A., LOOMANS M. E., LAHIRI S. K. and RÄISÄNEN I. Petri. Morphology and crystallization kinetics in HfO_2 thin films grown by atomic layer deposition. *Journal of Applied Physics*, 93:1477-1481, 2003.
- [27] CMi Machine - Neytech Qex Furnace.
<https://www.epfl.ch/research/facilities/cmi/equipment/packaging-miscellaneous/neytech-qex/>
- [28] PAYZANT, Edward. (2019). Re: "XRD for Si (100)?". Retrieved from:
<https://www.researchgate.net/post/What-is-the-difference-between-top-down-and-bottom-up-methods-for-creating-nano-structures/54ad3ce1cf57d73b448b46a8/citation/download>

Appendix

Final process flow

Lab : NEMS
 Operator Name : **Daniel Moreno / Andrea Elisei**
 Supervisor Name : Guillermo Villanueva
 Date of committee :

Téléphone : +41 21 693 85 04
 Office : MED 2 2726
 E-mail : daniel.moreno@epfl.ch

CMi EPFL Center of
 MicroNanoTechnology

Semestral Project Master Project Thesis Other

Flexoelectric NEMS

Description

Goal of project is to fabricate flexoelectric resonators based on high-k materials on the order of 100 nm in thickness. Note for process flow pictures: Checkered sections mean that layers are connected out-of-plane.

Technologies used			
<i>!! remove non-used !!</i>			
Positive resist, Development, Lift-off, ALD, Dry etching, Wet etching, Metrology, SEM, Dicing, Chip-level processing			
Photolithography masks			
Mask #	Critical Dimension	Critical Alignment	Remarks
1	10 um	First Mask	Bottom electrode liftoff
2	10 um	1 um	Top electrode definition
3	20 um	2 um	Electrode pad liftoff
4	2 um	1 um	Resonator release
Substrate Type			
Si test <100>, Ø100mm, Thickness 525 mm , p type, 0.1-100 Ohm.cm			

Lab : NEMS
 Operator Name : **Daniel Moreno / Andrea Elisei**
 Supervisor Name : Guillermo Villanueva
 Date of committee :

Téléphone : +41 21 693 85 04
 Office : MED 2 2726
 E-mail : daniel.moreno@epfl.ch

CMi EPFL Center of
 MicroNanoTechnology





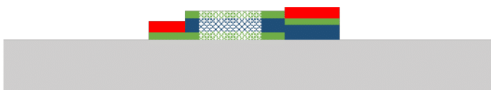
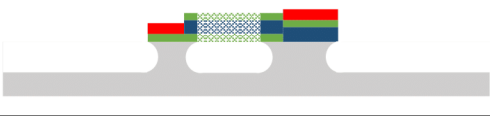
Process outline

Step	Process description	Cross-section after process
01	<i>Photolithography</i> Machine: EVG150 + MLA150 PR: LOR+AZ1512 Thickness: 0.48+1.1 um	
02	<i>Evaporation and liftoff</i> Machine: LAB600H PR: Z1 bench solvent in permanent baths Material: Cr + Pt Thickness: 2nm + 18nm Includes: <i>Descum O2 Plasma</i> (10s). Machine: Tepla	
03	<i>ALD / Evaporation</i> Machine: BENEQ/EVA 760 Material: HfO2 / Pt Thicknesses: - HfO2 : 25 or 50nm - Cr + Pt : 2nm + 18 nm	
04	<i>Photolithography</i> Machine: ACS200/MLA150 PR: AZ ECI3007 Thickness: 1 um	
05	<i>Dry/Wet Etching</i> Machine: IBE/HF Z2 Bench Material: Pt/HfO2 + Resist Strip	

Lab : NEMS
 Operator Name : **Daniel Moreno / Andrea Elisei**
 Supervisor Name : Guillermo Villanueva
 Date of committee :

Téléphone : +41 21 693 85 04
 Office : MED 2 2726
 E-mail : daniel.moreno@epfl.ch

CMi EPFL Center of
 MicroNanoTechnology

06	<p><i>Photolithography</i> Machine: EVG150 + MLA150 PR: LOR+AZ1512 Thickness: 0.48+1.1 um</p> <p>Includes: <i>Descum O2 Plasma</i> (10s). Machine: Tepla</p>	
07	<p><i>Evaporation and Liftoff</i> Machine: Lab 600/EVA 760 PR: Z1 bench solvent in permanent baths Material: Al Thickness: 500 nm</p>	
08	<p><i>Dicing of the samples</i> Machine: Dicer Disco DAD321 PR: Photoresist coating (AZ ECI) + dicing + Photoresist strip (remover 1165 Z2 UFT wet bench)</p>	
09	<p><i>Lithography</i> Machine: MLA PR: AZ ECI3007 Thickness: 1 um</p>	
10	<p><i>Dry Etching</i> Machine: STS Material: Pt/HfO2 +resist stripping</p>	
11	<p><i>Dry Release</i> Machine: AMS200 Etchant: SF6 Material: Si</p>	

After Step 09, the fabrication continues at the chip level to maximize the variety of actuators that can be fabricated.

